Developmental Cell
Article

A BBSome Subunit Links Ciliogenesis, Microtubule Stability, and Acetylation

Alexander V. Loktev,[1] Qihong Zhang,[2] John S. Beck,[2] Charles C. Searby,[2] Todd E. Scheetz,[2] J. Fernando Bazan,[1] Diane C. Slusarski,[3] Val C. Sheffield,[2] Peter K. Jackson,[1,*] and Maxence V. Nachury[1,4,*]
[1]Genentech, Inc., South San Francisco, CA 94080, USA
[2]Department of Pediatrics and Howard Hughes Medical Institute
[3]Department of Biology
University of Iowa, Iowa City, IA 52242, USA
[4]Department of Molecular and Cellular Physiology, Stanford University School of Medicine, Stanford, CA 94305, USA
*Correspondence: pjackson@gene.com (P.K.J.), nachury@stanford.edu (M.V.N.)
DOI 10.1016/j.devcel.2008.11.001

SUMMARY

Primary cilium dysfunction affects the development and homeostasis of many organs in Bardet-Biedl syndrome (BBS). We recently showed that seven highly conserved BBS proteins form a stable complex, the BBSome, that functions in membrane trafficking to and inside the primary cilium. We have now discovered a BBSome subunit that we named BBIP10. Similar to other BBSome subunits, BBIP10 localizes to the primary cilium, BBIP10 is present exclusively in ciliated organisms, and depletion of BBIP10 yields characteristic BBS phenotypes in zebrafish. Unexpectedly, BBIP10 is required for cytoplasmic microtubule polymerization and acetylation, two functions not shared with any other BBSome subunits. Strikingly, inhibition of the tubulin deacetylase HDAC6 restores microtubule acetylation in BBIP10-depleted cells, and BBIP10 physically interacts with HDAC6. BBSome-bound BBIP10 may therefore function to couple acetylation of axonemal microtubules and ciliary membrane growth.

INTRODUCTION

The primary cilium—a rod-like organelle present on the surface of most eukaryotic cells—has recently been the subject of much attention for its role in several signal transduction cascades, such as visual and olfactory sensation and the Sonic Hedgehog (Hh) morphogen pathway (Christensen and Ott, 2007; Scholey and Anderson, 2006). Notably, mice with mutations in the intraflagellar transport (IFT) machinery, which is necessary for building the cilium, display characteristic Hh signaling defects (Huangfu et al., 2003). At the cellular level, the Hh receptor Patched and the downstream transducer Smoothened respectively exit and enter the cilium during pathway activation (Corbit et al., 2005; Rohatgi et al., 2007).

A broader role for the primary cilium in cellular signaling is highlighted in a variety of pleiotropic hereditary disorders referred to as ciliopathies (Badano et al., 2006). In the example of Bardet-Biedl syndrome (BBS), patients suffer from obesity, retinopathy, anosmia, renal malformation, hypogenitalism, and polydactyly (Blacque and Leroux, 2006; Sheffield et al., 2004). Strikingly, studies in a variety of animal models have demonstrated that BBS proteins participate in the function of the primary cilium. For example, in zebrafish, knockdown of known BBS genes results in disruption of the Kupffer's vesicle (KV), a ciliated structure involved in left-right patterning (Chiang et al., 2006; Tayeh et al., 2008; Yen et al., 2006). Furthermore, worms harboring mutations in *bbs1*, *bbs7*, or *bbs8* fail to coordinate the movement of the two IFT subcomplexes inside the cilium (Ou et al., 2005, 2007). Altogether, the multitude of tissues and organs affected in BBS patients suggests defects in several tissue-specific ciliary signaling pathways.

We recently purified the BBSome—a stable complex of seven evolutionarily conserved BBS proteins—and proposed that it functions in ciliary membrane biogenesis (Nachury et al., 2007). First, the BBSome associates with the ciliary membrane; second, it binds to Rabin8, the guanosyl exchange factor for the small GTPase Rab8; third, $Rab8^{GTP}$ localizes to the cilium and promotes the docking and fusion of carrier vesicles to the base of the cilium. Thus, in one model, the BBSome directs vesicular trafficking to the cilium by modulating the ability of Rabin8 to activate Rab8. This model recently received support with the discovery that the ciliary membrane protein somatostatin receptor 3 fails to reach the cilium in hypothalamic neurons of *Bbs4* and *Bbs2* knockout mice (Berbari et al., 2008). Thus, the BBSome may function in the transport of specific proteins to the primary cilium.

Besides the ciliary membrane, the cilium consists of the axoneme, a radially symmetrical arrangement of 9 doublet microtubules (MTs). Interestingly, axonemal MTs are subject to post-translational modifications, including acetylation, detyrosination, and polyglutamylation (Westermann and Weber, 2003). Cytoplasmic and centrosomal MTs are also acetylated, and the acetylation of α-tubulin appears to take place after MT polymerization (Maruta et al., 1986). Therefore, acetylation seems to correlate with how long MTs have been available to serve as a substrate for the tubulin acetyltransferase (TAT), and a direct role for tubulin acetylation in MT dynamics seems unlikely (Palazzo et al., 2003). Our understanding of the enzymology of MT acetylation is limited to the identification of two tubulin deacetylases, HDAC6 and SIRT2, whereas the TAT remains to be discovered (Hubbert et al., 2002; North et al., 2003). Similarly to acetylated α-tubulin (ac-tubulin), detyrosinated α- and β-tubulin (Glu-tubulin) are markers of stable MTs and primary cilia (Johnson, 1998; Webster et al., 1987). Polyglutamylated α- and β-tubulin (polyglu-tubulin) can be detected on centrioles and axonemal MTs in most

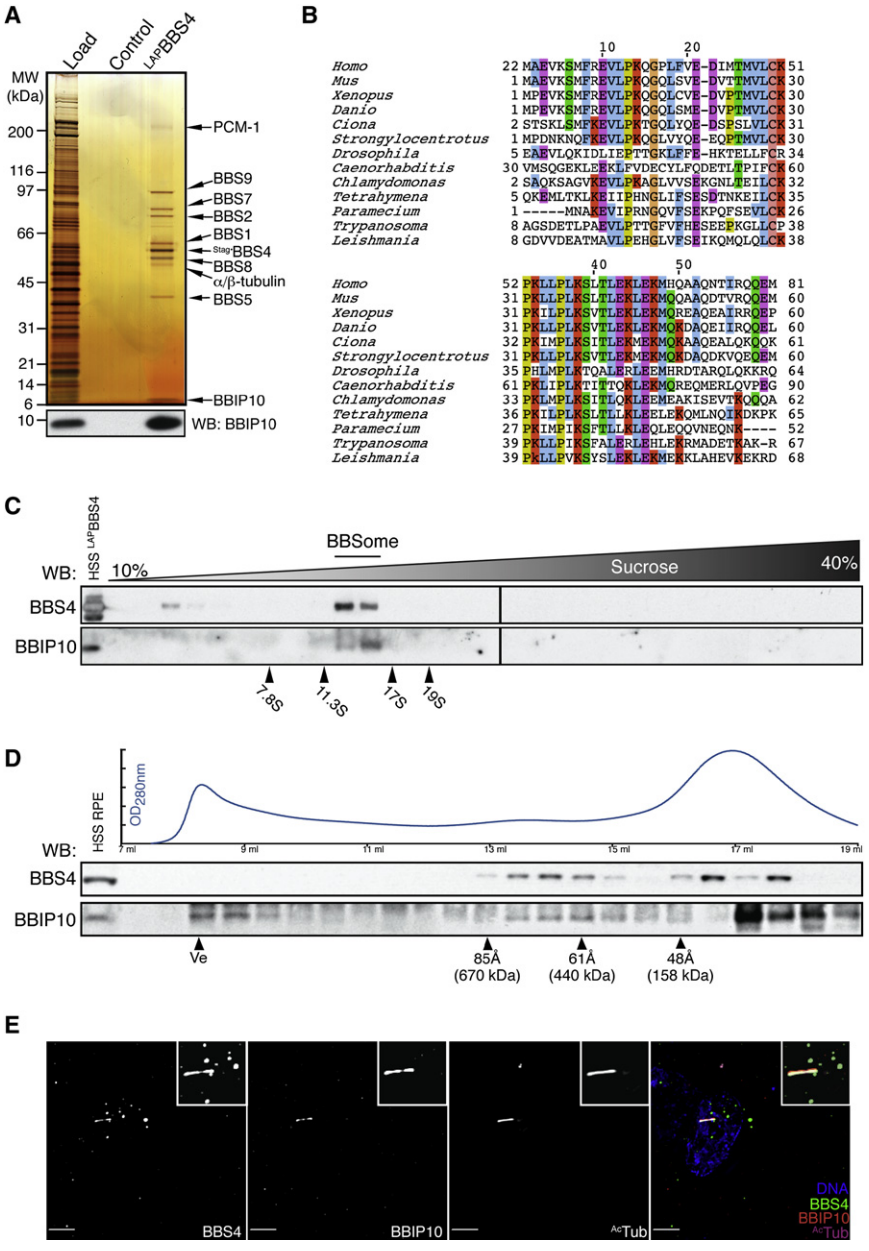

Figure 1. BBIP10 Is a BBSome Subunit

(A) BBIP10 copurifies with the BBSome. Tandem affinity purification of the BBS4 complex was performed, and eluates were resolved on a 4%–12% NuPAGE gel and silver stained. Proteins were identified by tandem mass spectrometry. Bottom panel: western blot of LAP-BBS4 purification eluates with BBIP10-specific antibodies.

(B) Partial multiple sequence alignment of BBIP10 orthologs found by reciprocal BLAST searches. Amino acid residues more than 30% identical are colored according to their biochemical properties. The entire alignment with Genebank accession numbers is presented in Figure S3.

(C) BBIP10 cosediments with the BBSome. LAP-BBS4 eluate was fractionated by sedimentation velocity on a linear 10%–40% sucrose density gradient. Fractions resolved on a 10% NuPAGE gel were blotted, and membranes were probed with anti-BBS4- and anti-BBIP10-specific antibodies. Sedimentation markers were fractionated simultaneously on an identical gradient, and their values were used to confirm the BBSome S value of 14.1S.

(D) BBIP10 partially cofractionates with the BBSome. RPE cell lysate was fractionated by size-exclusion chromatography and immunoblotted for BBS4 and BBIP10. The relative protein concentration is shown as OD_{280}. The excluded volume (Ve) and the elution volumes of individual Stokes radius markers are indicated. We note that some of BBS4 eluted at a molecular weight lower than the BBSome, which we have not observed previously in the similar analysis of mouse testes extract (Nachury et al., 2007).

(E) BBIP10 colocalizes with the ciliary pool of the BBSome. RPE-[^{LAP}BBS4] cells were immunostained for GFP, BBIP10, and ac-tubulin. Scale bars are 5 μm.

RESULTS

Discovery of a Novel BBSome Subunit

Following our discovery of the BBSome, we were interested in finding novel BBSome-associated proteins that may regulate or be effectors of its function. Careful examination of BBS4-interacting proteins, isolated by using tandem affinity purification from our previously described retinal pigmented epithelium (RPE) cell line stably expressing LAP-BBS4 used to purify the BBSome, revealed the presence of a 10 kDa polypeptide in near-stoichiometric amounts (Figure 1A) (Nachury et al., 2007). Tandem mass spectrometry identified this protein as the hypothetical product of the uncharacterized gene *LOC92482* (see Figure S1 available online). Remarkably, reciprocal BLAST searches yielded clear orthologs of LOC92482 in ciliated organisms (Figure S2), but not in plants, amoebae, or fungi. The LOC92482 protein sequence is well conserved in ciliated organisms; however, the primary sequence analysis did not reveal any conserved domains suggestive of its function (Figure 1B; Figure S3). Because of its association with the BBSome and functional overlap with BBS proteins

mammalian cells, and polyglutamylation has been shown to be important for cilia motility and centrosome stability (Bobinnec et al., 1998; Gagnon et al., 1996). The "tubulin code" model, analogous to the "histone code" hypothesis in epigenetics, posits that tubulin modifications modulate the binding of MT-associated proteins (MAPs) and motors to MTs, thus providing a mechanism for differential MAP and motor activity on distinct MT tracks (Bonnet et al., 2001; Reed et al., 2006; Verhey and Gaertig, 2007).

In this study, we describe a highly conserved subunit of the BBSome, which we name BBIP10. BBIP10 is required for primary cilium assembly, but, unexpectedly, it also functions to stabilize cytoplasmic MTs and maintain their acetylation. Given that these latter roles of BBIP10 do not overlap with BBSome function, we conclude that BBIP10, besides its crucial role in the BBSome, is a more global regulator of cytoplasmic MT stability.

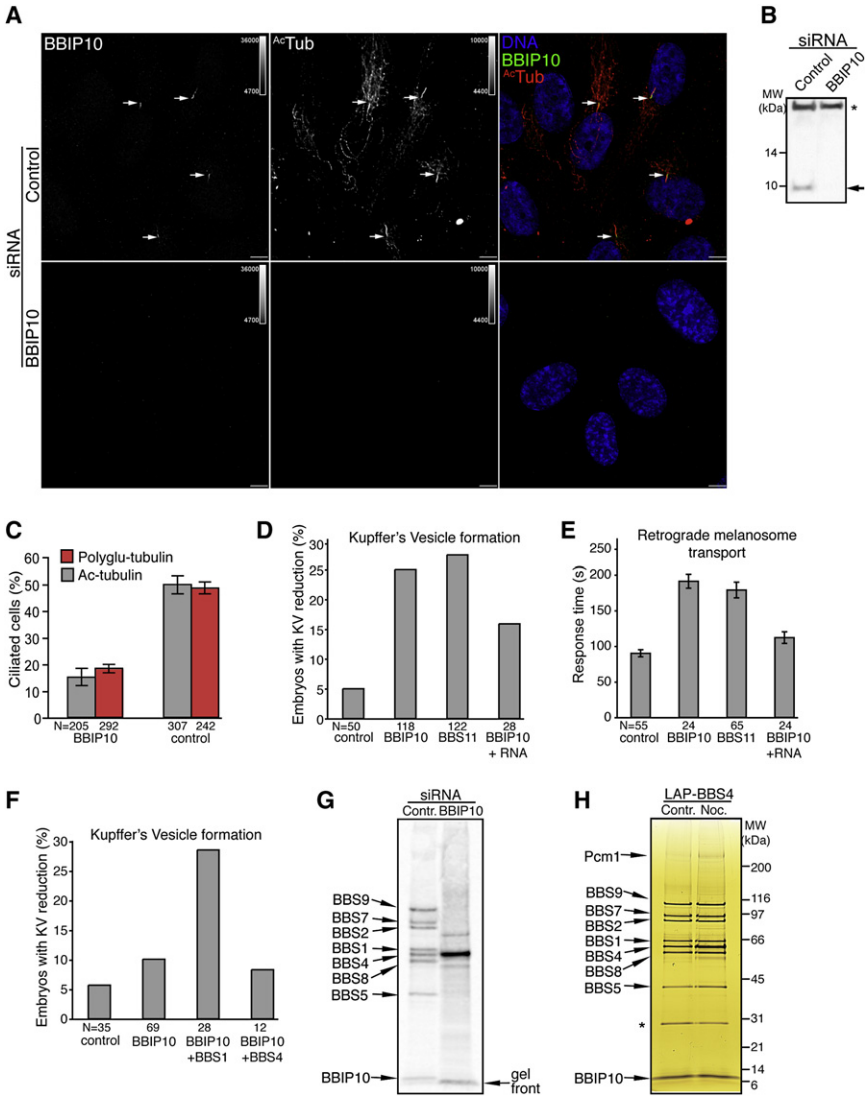

Figure 2. BBIP10 Is Essential for Ciliogenesis and BBSome Assembly

(A) BBIP10 is required for primary cilium formation in RPE cells. RPE cells were transfected with BBIP10 or control siRNA for 72 hr, serum starved for the last 48 hr, and fixed. Indirect immunofluorescence was performed with anti-BBIP10 and anti-ac-tubulin antibodies. Arrows indicate primary cilia. Scale bars are 10 μm.

(B) Validation of the anti-BBIP10 antibody by western blot. Whole-cell lysates of BBIP10 or control siRNA-transfected RPE cells were immunobloted for BBIP10 (band marked with an arrow). The nonspecific band marked with an astersik was used as a loading control. The complete blot is presented in Figure S4.

(C) Depletion of BBIP10 prevents ciliogenesis. RPE cells were prepared as in described in (A), stained for pericentrin and acetylated or polyglutamylated (GT335) tubulin. Cilia were counted in two independent experiments. Error bars represent SEM.

(D) BBIP10 depletion in zebrafish results in abnormal KV formation. Twenty five percent of the embryos had defects in KV morphology when injected with BBIP10 MO, whereas only 5% of control-injected embryos had such abnormalities. The phenotype could be rescued by coinjection of BBIP10 mRNA (100 ng/μl). BBS11 MO here and in (E) was used as a positive control for zebrafish BBS knockdown defects.

(E) BBIP10 morphants display delayed melanosome retraction. BBIP10 MO-injected embryos retracted melanosomes in 191 s, which is significantly ($p < 0.001$) delayed compared to 90 s in control-injected embryos. BBIP10 mRNA coinjection decreased transport time to 112 s in BBIP10 morphants. Error bars represent SD.

(F) BBIP10 genetically interacts with BBS1. Injection of a low dose of BBIP10 generates KV defects in 10% of embryos, whereas coinjection of a low dose of BBS1 MO with a low dose of BBIP10 MO increased the number of embryos with KV abnormalities to 28.6%. A low dose of BBIP10 coinjected with BBS4 MO did not produce such a change.

(G) The BBSome fails to form in the absence of BBIP10. The BBSome was purified by tandem affinity purification from [^{35}S]-methionine RPE-[^{LAP}BBS4] cells transfected with control or BBIP10 siRNA. Final eluates were resolved on a 4%–12% NuPAGE gel and blotted on PVDF membrane, which was exposed to a phosphostorage screen. The identity of the bands on the scan was inferred from comparison with a silver-stained gel (Figure 1A). The gel front is marked to help distinguish it from the BBIP10 band.

(H) Microtubules are not required for BBSome maintanence. RPE-[^{LAP}BBS4] cells were serum starved for 48 hr and treated with 0.16 μM nocodazole or DMSO control for 18 hr. The BBSome was isolated, resolved on a 4%–12% NuPAGE gel, and silver stained. The asterisk marks the contaminating TEV protease band.

(see below), we called this protein BBIP10 (BBSome Interacting Protein of 10 kDa).

To facilitate detection of endogenous BBIP10 in cells and cell extracts, we developed rabbit polyclonal antibodies against recombinant human BBIP10 (Figure 1A, bottom panel; Figure 2B; Figure S4). As a first step in characterizing this protein, we investigated the biochemical properties of its binding to the core BBSome (previously defined as the BBS1, -2, -4, -5, -7, -8, and -9 complex). We subjected the native LAP-BBS4 eluate to velocity sedimentation analysis (Figure 1C). BBIP10 clearly cosedimented with BBS4 at 14S, suggesting that BBIP10 strongly associates with the core BBSome, unlike the loosely bound PCM-1 (Nachury et al., 2007). We previously showed that all core BBSome subunits exclusively cofractionate in gel filtration of mouse testes lysate. Since our anti-BBIP10 antibody did not detect the mouse BBIP10 ortholog (data not shown), we used gel filtration of RPE cell lysate to investigate BBIP10's association with the BBSome. A portion of BBIP10 clearly cofractionated with BBS4 at ~440 kDa (61 Å) (Figure 1D). Still, we note that the bulk of BBIP10 eluted in low-molecular weight fractions with unknown protein partners.

Next, we used our anti-BBIP10 antibody to visualize BBIP10 in human RPE cells, a well-established system for studying ciliogenesis (Mikule et al., 2007; Pugacheva et al., 2007). Remarkably, BBIP10 colocalized precisely with BBS4 inside the primary cilium, but not at centriolar satellites (Figure 1E). This localization

pattern suggests that BBIP10 associates with the BBSome inside the primary cilium, but not at centriolar satellites, where the BBSome is bound to PCM-1.

BBIP10 Is Required for the Primary Cilium Formation

The evolutionary conservation of BBIP10, its binding to the BBSome, and its localization to the cilium motivated us to examine the contribution of BBIP10 to primary cilium formation in RPE cells. Three different siRNA oligonucleotides reduced BBIP10 mRNA levels by greater than 91% and rendered BBIP10 protein undetectable by immunoblotting and immunostaining (Figures 2A and 2B; Figure S5A). Remarkably, the extent of BBIP10 knockdown correlated with a dramatic decrease in ciliation, indicating that BBIP10 is essential for ciliogenesis (Figures 2A and 2C; Figure S5B). Unexpectedly, we also observed a marked reduction in cytoplasmic MT acetylation (Figure 2A). The absence of cilia in BBIP10-depleted cells was therefore confirmed by using an independent marker of the ciliary axoneme, polyglu-tubulin (Figure 2C).

Having established the requirement for BBIP10 in ciliogenesis in tissue culture cells, we next examined the effect of BBIP10 loss of function in an animal model. Interference with BBS gene function in zebrafish embryos is known to result in two specific phenotypes: malformation of the KV and a delay in retrograde melanosome transport (Chiang et al., 2006; Tayeh et al., 2008; Yen et al., 2006). First, analogous to the node in mammals, the KV is an embryonic ciliated structure involved in left-right asymmetry determination in fish. Embryos injected with BBIP10 morpholino oligonucleotides (MO) displayed KV abnormalities five times more frequently than control animals (Figure 2D). This effect was specific since it could be rescued by coinjection of BBIP10 mRNA along with the MO (Figure 2D). Second, melanosomes undergo retrograde translocation from the cell periphery to the perinuclear region in response to light and epinephrine, which can be assayed as a function of time. The retrograde transport of melanosomes was slowed down to a similar extent by injection of MOs targeting *bbip10*, *bbs11* (Figure 2E), or *bbs2* (data not shown). The defect brought about by BBIP10 MO could be rescued by coinjection of BBIP10 mRNA (Figure 2E). We previously determined subphenotypic doses of BBS1 and BBS4 MOs that do not generate substantial KV defects or melanosome trafficking delays (Tayeh et al., 2008). Injection of a low dose of BBIP10 MO alone caused only a slight increase in KV defects. However, coinjection of a low-dose combination of BBIP10 and BBS1 MOs showed a dramatic increase in KV abnormalities, whereas combined injections of BBIP10 and BBS4 MOs did not alter KV defects relative to individual exposure (Figure 2F). Thus, BBIP10-depleted zebrafish embryos display characteristic BBS phenotypes, and BBIP10 genetically interacts with BBS1.

Correlation of gene expression has been demonstrated to be a powerful method for identifying coregulated genes within a molecular pathway (Eisen et al., 1998). We therefore analyzed *Bbip10* expression relative to 11 BBS genes in a rat eQTL experiment (Scheetz et al., 2006). As validation of this method, the data set was previously exploited to identify *TRIM32* as *BBS11* (Chiang et al., 2006). *Bbip10* expression was found to strongly correlate with the expression of the other BBS genes (Figure S6). Thus, together with the data showing BBIP10 binding to the BBSome, its localization to the cilium, and the requirement for BBIP10 in cilium assembly, these data demonstrate that BBIP10 is an important component of the BBS pathway. We note however, that no mutations in the *BBIP10* coding sequence could be identified in a panel of over 300 BBS probands without mutation in known BBS genes. Thus, BBIP10 may carry out functions beyond the BBS pathway, or, alternatively, the small size of the *BBIP10* gene may make it a limited target for spontaneous mutations and a very rare cause of BBS.

BBIP10 Is Required for the Assembly of the BBSome

Given the substantial overlap between the functions of BBIP10 and the other BBSome subunits, we wanted to understand if BBIP10 might function in BBSome assembly. We assayed BBSome assembly by metabolic labeling and purification of the BBS4-associated complex after depletion of BBIP10 by siRNA. Remarkably, we could not detect any BBSome subunits copurifying with BBS4, suggesting that BBS4 fails to incorporate into the BBSome in the absence of BBIP10 (Figure 2G). The potential role of several BBS proteins, and BBIP10 in particular (see below), in MT-related processes prompted us to ask whether MTs in general are required for the maintenance of the BBSome. To address this question, we purified the BBSome from cells treated with the MT depolymerization agent nocodazole. Prior to drug treatment, cells were serum starved to induce ciliation and to avoid mitotic arrest due to the engagement of the spindle assembly checkpoint. The subunit composition of the BBSome purified from cells without MTs was indistinguishable from the control (Figure 2H). Thus, we conclude that BBIP10 is likely to play a direct role in BBSome assembly.

Systematic Analysis of BBS Protein Function in Microtubule-Based Processes

The striking effect of BBIP10 depletion on ciliogenesis and MT acetylation led us to question whether the BBSome itself influences these processes. Although BBS proteins have been proposed to be important for MT- and centrosome-based functions, direct evidence for these roles in mammalian cells remains limited. BBS4 has been implicated in MT-based transport of centriolar satellites via its interaction with PCM-1 and the dynein/dynactin motor complex (Kim et al., 2004), and BBS6 has been localized to centrosomes (Kim et al., 2005). To uncover potential functional overlap among the 12 known BBS proteins, BBIP10, and PCM-1, we undertook a systematic analysis of MT-based processes upon depletion of these proteins in RPE cells. We chose to analyze cilium formation, centrosome morphology, BBS4 localization, and MT acetylation. In particular, we were interested in finding phenotypic differences between BBIP10-depleted cells and cells lacking individual BBS proteins.

We found that the ability of RPE cells to ciliate was dramatically decreased by knockdown of BBIP10, BBS1, BBS5 and PCM-1 (Figures 3A and 3B; Figure S7), whereas ciliation in cells depleted of all other BBS proteins was not substantially different from the control. This is not surprising given that all BBS knockout mice generated so far (*Bbs2*, *Bbs4*, and *Bbs6*), as well as a BBS1M390R knockin mouse model, are able to form cilia (Davis et al., 2007; Fath et al., 2005; Mykytyn et al., 2004; Nishimura et al., 2004). None of the knockdowns besides BBIP10 appeared to have a dramatic effect on cytoplasmic ac-tubulin staining (Figure 3A).

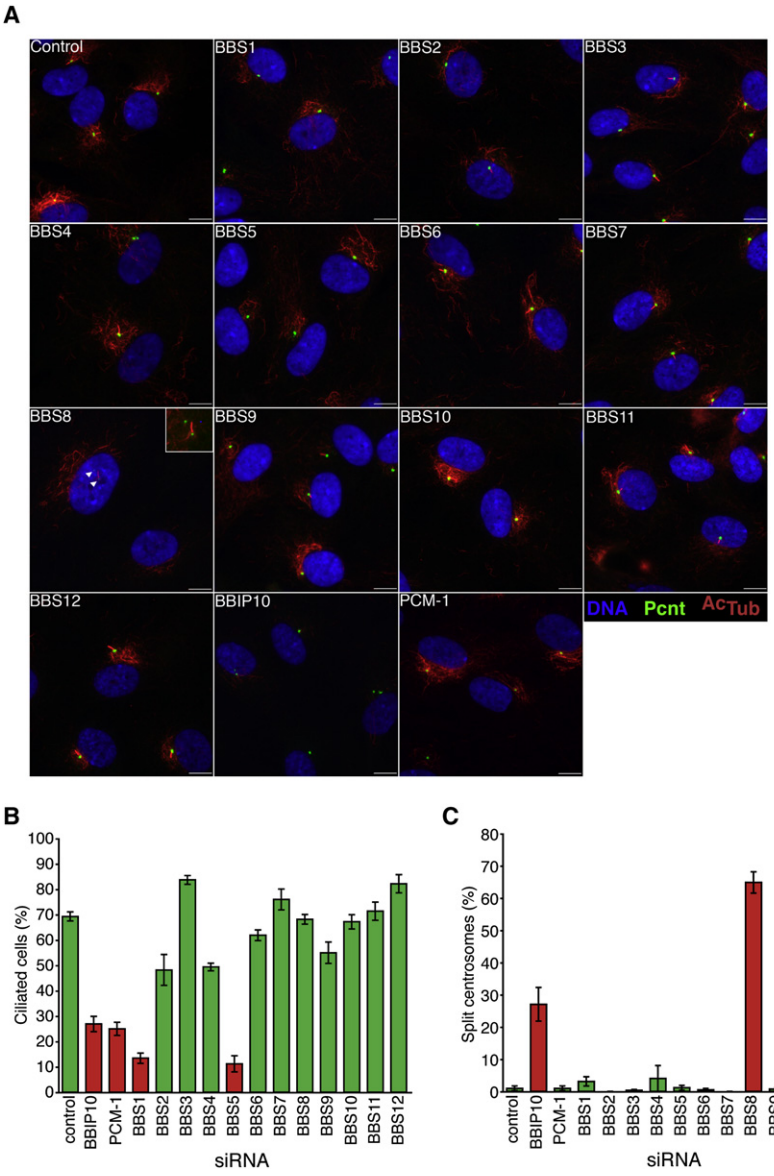

Figure 3. Analysis of Ciliogenesis and Centrosome Morphology upon Depletion of Individual BBS Proteins by siRNA

(A) Analysis of ciliogenesis, centrosome splitting, and tubulin acetylation upon BBS protein depletion. RPE cells transfected with indicated siRNAs for 72 hr and serum starved for the last 48 hr were fixed and stained for pericentrin (green), ac-tubulin (red), and DNA (blue). Split centrioles in BBS8-depleted cells are marked with arrowheads. Merged representative images are presented. Validation of the specific mRNA depletion by qRT-PCR is presented in Figure S7. Scale bars are 10 μm.

(B) A ciliogenesis assay in RPE cells depleted of BBS proteins by siRNA. RPE cells were siRNA transfected and processed as in (A). Cilia were counted in two independent experiments. Error bars represent SEM.

(C) Quantitation of centrosome splitting in BBS-depleted RPE cells. The same samples as in (B) were analyzed for centrosome splitting. Centrosome integrity was scored as compromised when two or more pericentrin foci at least 2 μm apart were observed in a single cell (red bars). Only interphase cells, as defined by noncondensed DNA staining, were counted. Error bars represent SEM.

Surprisingly, depletion of BBIP10 and BBS8 caused a dramatic increase in the frequency of centrosome splitting in interphase cells (Figures 3A and 3C). Interestingly, the levels of pericentrin staining at the centrosome were dramatically reduced in BBS8-depleted cells, but not in BBIP10-depleted cells, (Figure 3A). Since pericentrin has been shown to be required for primary cilia assembly (Jurczyk et al., 2004; Mikule et al., 2007), we were surprised to find that cells lacking BBS8 were able to grow cilia despite a drastic reduction in pericentrin levels at the centrosome and split centrosomes. Taken together, these observations argue against centrosome splitting being the primary cause of ciliogenesis defect found in BBIP10-depleted cells (also see Graser et al., 2007).

It was of interest to investigate if BBIP10 depletion would affect BBS4 localization to centriolar satellites given that BBS4 fails to incorporate into BBSome in the absence of BBIP10. We found, however, that BBS4 remained localized to centriolar satellites in BBIP10-depleted cells (Figure S9). Notably, none of the siRNA treatments except for PCM-1 caused mislocalization of BBS4 from centriolar satellites (data not shown).

Although other BBSome subunits are found to be required for cilium formation, centrosome cohesion, centriolar satellite distribution and MT organizing center integrity (Figure S8), BBIP10 is the only subunit for which our experiments have been able to identify a role in cytoplasmic MT acetylation. It is therefore likely that BBIP10 participates in this process in a BBSome-independent manner.

BBIP10 Regulates Microtubule Polymerization

Although acetylation of Lys40 of α-tubulin has been widely used as a marker for the primary cilium, acetylated MTs are also found in the cytoplasm (Piperno et al., 1987). An intriguing absence of acetylated cytoplasmic MTs in BBIP10-depleted cells and the apparent lack of this phenotype among other BBSome subunit knockdowns motivated us to examine it in more detail (Figures 2A, 3A, and 4A). Furthermore, in BBIP10-depleted cells, the density of cytoplasmic MTs was dramatically diminished and the levels of unpolymerized α-tubulin were increased (Figure 4B). Thus, BBIP10 is required for MT stabilization in vivo, and the decrease in MT acetylation found in BBIP10-depleted cells may be an indirect consequence of global MT destabilization. If the loss of acetylated MTs is merely a by-product of the decrease in

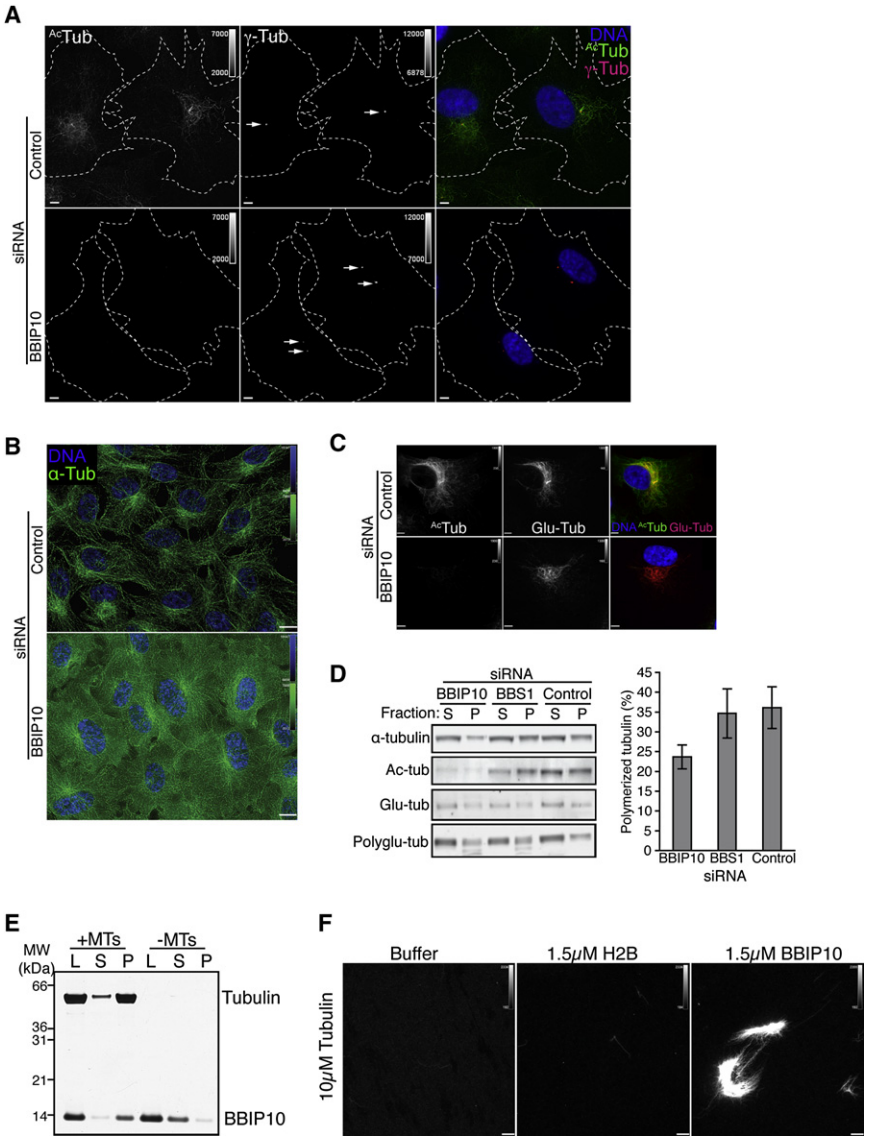

Figure 4. Loss of BBIP10 Affects Microtubule Stability and Centrosome Splitting

(A) BBIP10 depletion results in a loss of acetylated microtubules and split centrosomes. RPE cells depleted of BBIP10 and control cells were stained for ac-tubulin and γ-tubulin. Arrows point to centrosomes. Scale bars are 5 μm.

(B) BBIP10 depletion results in an increase in depolymerized tubulin. RPE cells depleted of BBIP10 and control cells were fixed with 4% PFA to preserve soluble tubulin and immunostained for α-tubulin. Scale bars are 10 μm.

(C) Detyrosinated tubulin staining is unaffected in BBIP10-depleted cells. RPE cells transfected with BBIP10 or control siRNA were stained for Glu-tubulin and ac-tubulin. Scale bars are 5 μm.

(D) Microtubule acetylation is specifically affected in BBIP10-depleted cells. Left panel: polymerized (P) and soluble (S) pools of tubulin from BBIP10, BBS1, or control siRNA-treated cells were separated as described in Experimental Procedures and were analyzed by quantitative immunoblotting for total α-tubulin and tubulin modified by acetylation, polyglutamylation, and detyrosination (Glu-tubulin). Right panel: percentage of α-tubulin in the P fraction was plotted based on two independent experiments performed in triplicate. Error bars represent SEM.

(E) BBIP10 copellets with taxol-stabilized microtubules. Pure tubulin (4 μM), polymerized by the addition of taxol, was incubated with purified recombinant His-BBIP10 (3 μM) and centrifuged through a glycerol cushion. Equivalent amounts of load (L), supernatant (S), and pellet (P) were resolved on a 12% NuPAGE gel and silver stained. The amounts of recovered tubulin and BBIP10 in S+P fractions are similarly reduced due to a loss of proteins in the glycerol cushion during centrifugation.

(F) BBIP10 directly promotes microtubule polymerization in vitro. The addition of His-BBIP10 (1.5 μM) to tubulin (10 μM), supplemented with Rhodamine-labeled tubulin (0.5 μM), induced assembly of aster-like microtubule structures, unlike histone H2B (1.5 μM) or tubulin alone. Scale bars are 5 μm.

stable MTs, other markers of stable MTs, i.e., Glu-tubulin and polyglu-tubulin, should also disappear in BBIP10-depleted cells. However, in contrast to ac-tubulin, we did not observe a reduction in overall staining intensity for these two markers in BBIP10-depleted cells (Figure 4C, data not shown). The decreased MT stability and the loss of MT acetylation were further validated biochemically in a MT-pelleting assay. Since BBS1 is required for ciliation and interacts genetically with BBIP10, we used BBS1 siRNA as a specificity control to test whether the role of BBIP10 in MT stabilization is related to a general BBSome function or is specific to BBIP10 (Figures 2F and 3B). Consistent with the immunofluorescence analysis, MTs from BBIP10-depleted cells had greatly diminished acetylation, but detyrosination and polyglutamylation remained unperturbed (Figure 4D). The percentage of α-tubulin found in the pellets, i.e., polymerized tubulin, was also significantly reduced in BBIP10-depleted cells (Figure 4D). The depletion of BBS1 did not affect either MT acetylation or polymerization, suggesting that BBIP10 functions in MT stabilization and acetylation independently of the BBSome (Figure 4D).

Additionally, greater than 30% of cells lacking BBIP10 had two or more foci of pericentrin or γ-tubulin staining (separated by >2 μm) compared to 1% of control cells (Figures 3C and 4A), suggesting that BBIP10 is required for centrosome cohesion. This observation was confirmed by cotransfecting BBIP10-depleted cells with RFP-centrin 2, a marker of the individual centrioles (Figure S10).

The above-described results put forward the hypothesis that BBIP10 acts directly on MTs. To determine if BBIP10 directly binds MTs, we turned to in vitro assays with recombinant BBIP10 and purified bovine brain tubulin. In support of the above-described hypothesis, BBIP10 efficiently copelleted with taxol-stabilized MTs but remained in solution without MTs (Figure 4E). Additionally, incubation of fluorescently labeled tubulin with BBIP10 led to the formation of MT asters, whereas tubulin alone or with a control protein failed to polymerize (Figure 4F). The

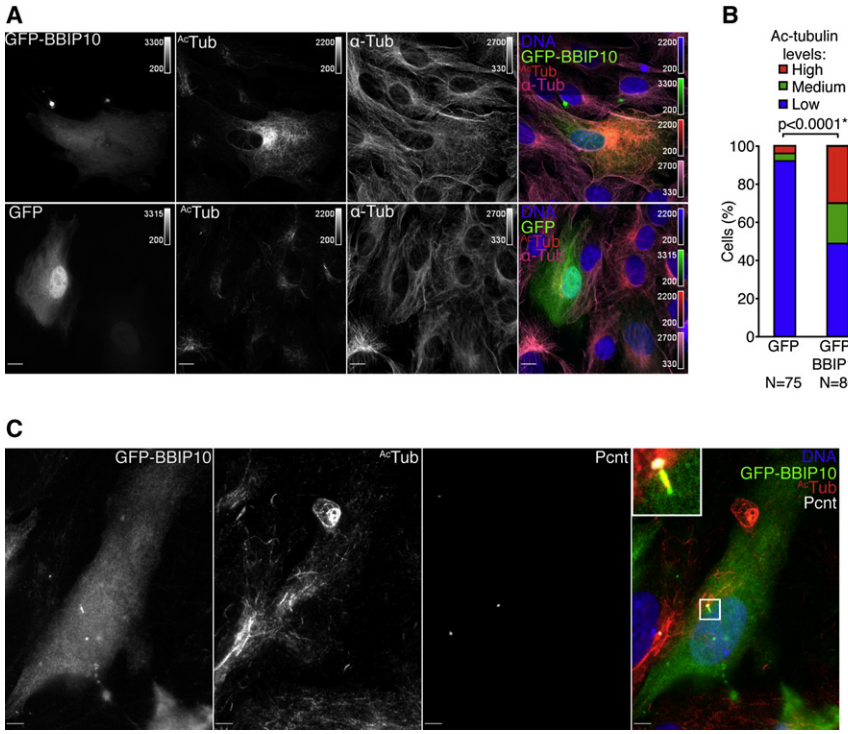

Figure 5. BBIP10 Overexpression Promotes Microtubule Hyperstabilization

(A) BBIP10 overexpression promotes microtubule hyperstabilization. RPE cells were transfected with GFP-BBIP10 or control vector for 48 hr, fixed, and stained for ac-tubulin and α-tubulin. Scale bars are 5 μm.

(B) Ac-tubulin staining in GFP- or GFP-BBIP10-expressing cells was scored as low, medium, or high and plotted. A chi-square test was used to test the statistical difference between the two distributions ($p < 0.0001$).

(C) Ectopically expressed GFP-BBIP10 localizes to the primary cilium in RPE cells. RPE cells were transfected with GFP-BBIP10 for 24 hr, serum starved for an additional 24 hr, fixed, and stained for ac-tubulin and pericentrin. Cells expressing low levels of GFP-BBIP10 were selected for imaging. A representative image is shown. Scale bars are 5 μm.

concentration of BBIP10 used in this experiment is similar to the amounts reported for the well-characterized MAP TPX2 (Schatz et al., 2003). Thus, these data suggest that BBIP10 directly binds and stabilizes MTs in vitro.

BBIP10 Overexpression Drives Microtubule Acetylation

Since depletion of BBIP10 caused a dramatic reduction in α-tubulin acetylation, we reasoned that overexpression of the protein in cells might promote MT stabilization and acetylation. Indeed, cells expressing moderate levels of GFP-BBIP10 frequently had dramatically increased levels of ac-tubulin staining (Figures 5A and 5B). Furthermore, overexpression of a siRNA-resistant variant of BBIP10 rescued tubulin acetylation in BBIP10-depleted cells (Figure S11). Surprisingly, no clear staining of GFP-BBIP10 was found on MTs. This could be explained by an inhibition of binding between BBIP10 and MTs in vivo similarly to conventional kinesin, a classical MAP that does not localize to MTs in cells (Lippincott-Schwartz et al., 1995; Vale et al., 1985). Nonetheless, in serum-starved RPE cells, GFP-BBIP10 was easily detected in the primary cilium, consistently with BBIP10 antibody staining (Figure 5C; Figure S12).

BBIP10 Influences Microtubule Acetylation Independently of Microtubule Stabilization

Since BBIP10 appears to be sufficient to promote MT stabilization in vitro, is it required for MT assembly in cells? To answer this question, we used live-cell imaging to follow MT regrowth in cells recovering from nocodazole treatment. Surprisingly, no significant differences were observed in the rates of MT regrowth from the centrosome between BBIP10-depleted and control-depleted cells (Figure 6A; Movies S1 and S2). Interestingly, split centrioles in BBIP10-depleted cells appeared to be able to nucleate MTs, but lost the ability to anchor them (Figure 6A; Movies S1 and S2).

MT acetylation has been shown to closely follow MT reassembly after nocodazole recovery (Piperno et al., 1987). We found that MTs were not acetylated at any time points in BBIP10-depleted cells even though the kinetics of tubulin polymerization were not dramatically perturbed (Figures 6B and 6C). Since MTs become acetylated postassembly, stabilization of MTs by taxol or the overexpression of MAPs effectively drives acetylation (Piperno et al., 1987; Takemura et al., 1992). We therefore used taxol treatment to test whether the requirement for BBIP10 in acetylation is separate from its MT-stabilizing function. As expected, control-depleted cells accumulated ac-tubulin with increasing concentrations of taxol. In contrast, the levels of tubulin acetylation in BBIP10-depleted cells remained low regardless of the taxol concentration (Figure 6D). Quantitative biochemical analysis confirmed that forced polymerization of MTs by taxol in cells fails to rescue MT acetylation in BBIP10-depleted cells (Figures 6E and 6F). Interestingly, we observed slightly more Glu-tubulin in BBIP10-depleted cells than in control cells after taxol treatment, whereas no significant difference was detected in the case of polyglutamylation (Figures 6E and 6F). Taken together, these data strongly suggest that BBIP10 controls tubulin acetylation independently of MT polymerization.

HDAC6 Inhibition Rescues Tubulin Acetylation in BBIP10 Knockdown

Having established that the defect in tubulin acetylation upon BBIP10 depletion is not dependent on MT polymerization, we tested if enzymes known to be involved in tubulin acetylation are implicated in the BBIP10 phenotype. Because recent evidence suggests that HDAC6 is the predominant enzyme that deacetylates tubulin, we tested if inhibiting HDAC6 activity rescues the lack of tubulin acetylation in cells (Zhang et al., 2008). Inhibition of HDAC6 activity with the specific small molecule inhibitor

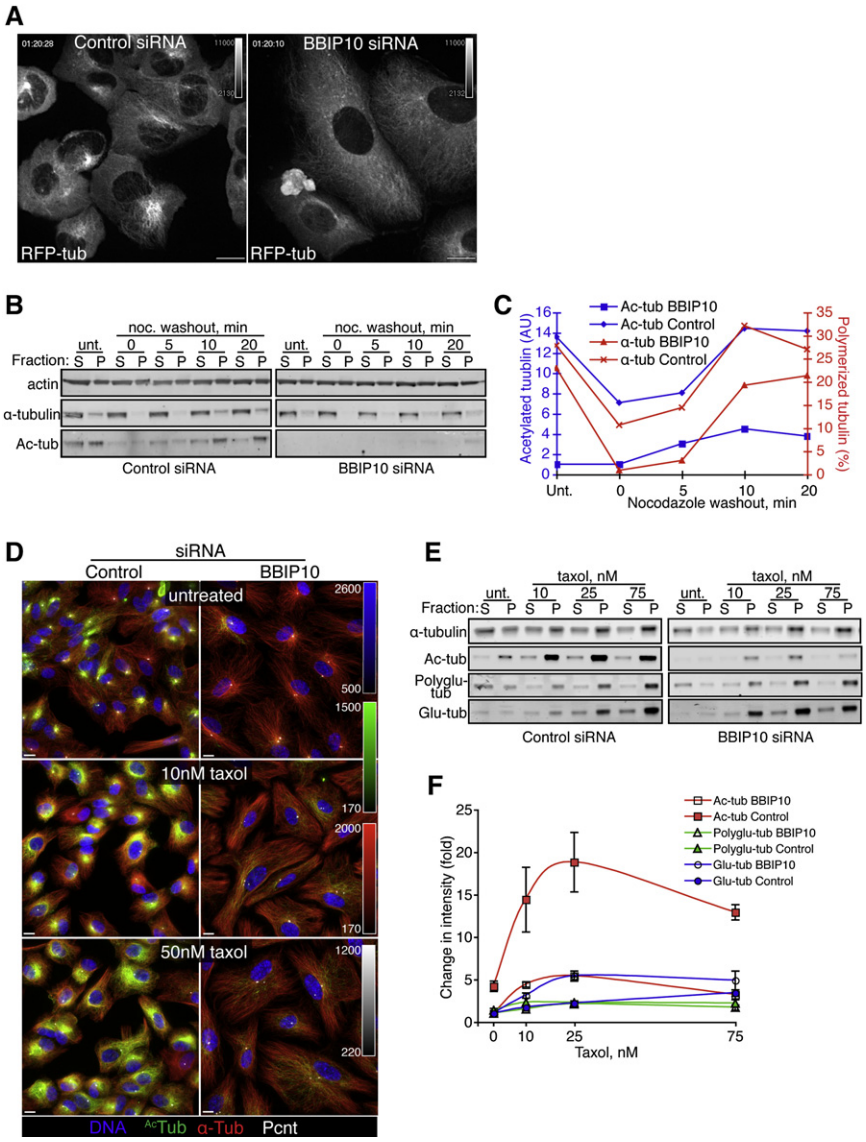

Figure 6. Microtubule Stabilization Does Not Rescue the Acetylation Defect in BBIP10-Depleted Cells

(A) Microtubule anchoring at the centrosome is defective in BBIP10-depleted cells. U-205 cells stably expressing RFP-tubulin were transfected with control or BBIP10 siRNA for 72 hr. Microtubules were imaged by using time-lapse microscopy during treatment with 0.5 μM nocodazole, followed by washout. The final frame of each of the time-lapse series is presented. Scale bars are 10 μm. Complete movies are available in Supplemental Data.

(B) Microtubules are not acetylated upon reassembly de novo in BBIP10-depleted RPE cells. BBIP10 or control siRNA-transfected cells were treated with 0.5 μM nocodazole for 1 hr, the drug was washed out, and cells were processed as in Figure 3D at the indicated time points. The intensity of ac-tubulin bands in the pellet (P) fractions and the percentage of the tubulin in the pellets were quantified and plotted in the graph shown in (C). Unt., untreated; AU, arbitrary units.

(D) Taxol-stabilized microtubules are not acetylated in BBIP10-depleted RPE cells. BBIP10 or control siRNA-transfected cells were treated with indicated concentrations of taxol for 1 hr, fixed, and immunostained for ac-tubulin, α-tubulin, and pericentrin.

(E) Taxol-driven microtubule acetylation is defective in BBIP10-depleted cells. BBIP10 or control siRNA-transfected cells were treated with increasing concentrations of taxol for 1 hr and processed as in Figure 3D. The intensities of ac-, polyglu-, and Glu-tubulin bands in the P fractions were measured. Changes in signal were quantified by dividing by the intensity of the band in the BBIP10 siRNA-untreated sample. The change in intensities was plotted as a function of taxol concentration and shown in (F). Measurements presented are from two independent experiments performed in triplicate. Error bars represent SEM. Unt., untreated.

tubacin partially restored levels of tubulin acetylation in BBIP10-depleted cells, whereas treatment with the inactive derivative niltubacin had no effect (Figures 7A and 7B) (Haggarty et al., 2003). To confirm that the rescue of tubulin acetylation is due to HDAC6 inhibition, we performed double knockdown of BBIP10 and HDAC6 by siRNA and obtained similar results (Figure 7C). Moreover, we found that BBIP10 specifically interacts with HDAC6 when cotransfected in cells (Figure 7D). These data suggest that BBIP10 might affect tubulin acetylation status by inhibiting HDAC6.

DISCUSSION

There is a considerable interest in further defining the molecular pathways leading to BBS and other ciliopathies. Our approach to understanding the molecular pathomechanisms of BBS has been to look for novel BBSome-associated proteins. This led us to the identification of a BBSome subunit – BBIP10. Here, we show that BBIP10 (1) cofractionates stoichiometrically and coimmunoprecipitates with the BBSome; (2) colocalizes with the BBSome to the primary cilium, but not to satellites; (3) is required for primary cilia assembly and BBSome stability; and, most surprisingly, (4) regulates MT stability and acetylation in vivo.

BBSome-Dependent and BBSome-Independent Functions of BBIP10

Is the role of BBIP10 in the regulation of cytoplasmic MTs related to its ciliogenic function? Systematic assessment of five distinct parameters in BBS-depleted cells allowed us to conclude that the phenotype of BBIP10 knockdown shows extensive overlap with other BBS proteins with some crucial differences. Whereas several BBS proteins, like BBIP10, are required for ciliogenesis, centrosome cohesion, or MT organizing center activity, none of them impinges upon cytoplasmic MT stability and acetylation.

BBIP10 appears to be present in at least two distinct fractions: a 470 kDa fraction corresponding to the BBSome and a < 100 kDa low-molecular weight fraction. Immunofluorescence data suggest that the interaction between BBIP10 and the BBSome

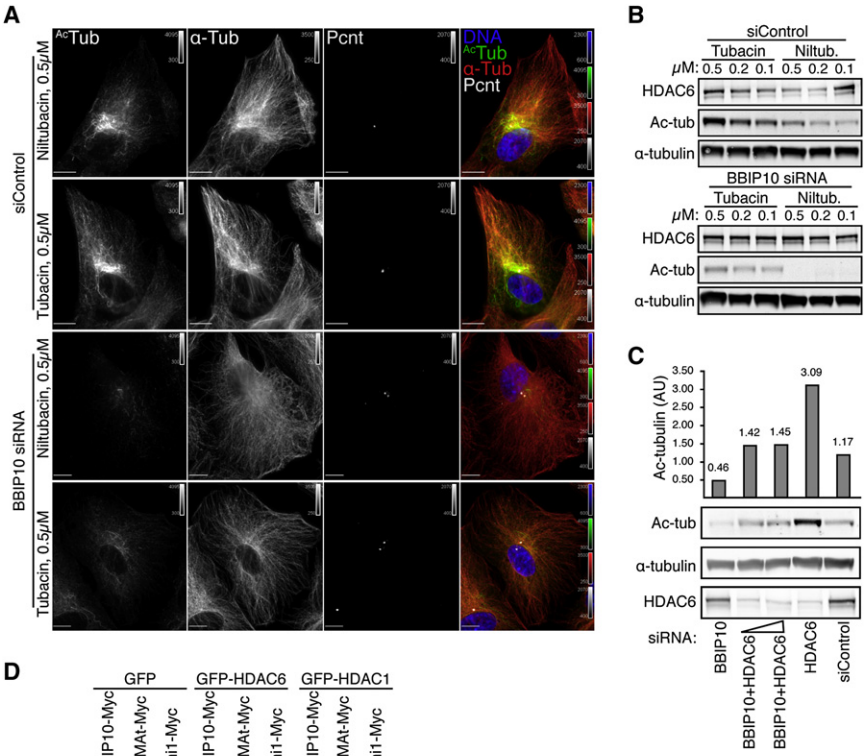

Figure 7. Tubulin Acetylation in BBIP10-Depleted Cells Is Rescued by Inhibiting HDAC6

(A) Inhibiting HDAC6 with tubacin partially rescues microtubule acetylation in cells lacking BBIP10. RPE cells transfected with BBIP10 or control siRNAs for 72 hr were treated with 0.5 μM tubacin or niltubacin for 4 hr, fixed, and stained for ac-tubulin, α-tubulin, and pericentrin. Scale bars are 10 μm.

(B) Western blot of cells treated as described above with varying concentrations of tubacin and niltubacin.

(C) Depleting HDAC6 by siRNA partially rescues microtubule acetylation in cells lacking BBIP10. Lysates from RPE cells transfected with BBIP10 (50 nM) and HDAC6 (50 nM) siRNAs separately or together (25 nM each or 50 nM each) for 72 hr were blotted for ac-tubulin, α-tubulin, and HDAC6. The intensities of ac-tubulin bands were measured, normalized to intensities of corresponding α-tubulin bands, and plotted.

(D) BBIP10 interacts with HDAC6. 293T cells were cotransfected with expression constructs for 48 hr as indicated. GFP immunoprecipitates were blotted for GFP and myc tag. WCL, whole-cell lysate. GFP-HDAC1, NuMAt, and Emi1-Myc were used as specificity controls.

occurs in the primary cilium, whereas the other pool of BBIP10 is distributed diffusely in the cytoplasm. It seems likely that the cytoplasmic (i.e., non-BBSome bound) population of BBIP10 regulates MT stabilization and acetylation. However, in analyzing the function of an individual protein, which is also a subunit of a multiprotein complex, we wanted to take into account the function of the entire complex. Since the BBSome assembly is compromised in the absence of BBIP10, we cannot properly distinguish at this time between phenotypes stemming from loss of the BBSome or loss of BBIP10. For example, we cannot exclude that the compromised BBSome assembly is the cause of the MT acetylation defect in BBIP10 knockdown. It is tempting to speculate that the failure in ciliogenesis of BBIP10-depleted cells is due, at least in part, to the incomplete BBSome assembly. The data that the BBSome composition is normal in the absence of MTs strongly argue that its assembly takes place in the cytoplasm independently of MTs. This places BBIP10 upstream of both BBSome assembly and MT stability and acetylation. Additional studies are in progress to discover the mechanism and requirements for the BBSome assembly and its relevance to the function of the primary cilium.

How Does BBIP10 Influence Microtubule Acetylation?

Cells lacking BBIP10 have dramatic alterations in their MT cytoskeleton, namely, an absence of acetylated cytoplasmic MTs and decreased MT polymerization. To date, the functional consequences of tubulin acetylation remain quite elusive. Genetic introduction of an α-tubulin gene resistant to acetylation at Lys40 in *Tetrahymena* and *Chlamydomonas* demonstrates that acetylation is not essential for survival or ciliation in these organisms (Gaertig et al., 1995; Kozminski et al., 1993). However, more recent data suggest that Kinesin-1 preferentially utilizes acetylated MT tracks for its movement (Reed et al., 2006). Our data strongly suggest that BBIP10 regulates tubulin acetylation independently of its MT-stabilizing properties. This led us to postulate that BBIP10 inhibits HDAC6; however, BBIP10 does not appear to inhibit HDAC6 directly in our initial in vitro assays (data not shown). The rescue of tubulin acetylation by inhibition of HDAC6 does not rule out that BBIP10 might be required for the activity of the TAT. Suppressing HDAC6 activity in cells lacking BBIP10 might be sufficient for the residual TAT activity to catalyze detectable tubulin acetylation, which, in the absence of reverse reaction, appears as a partial rescue.

To date, there is no evidence of biochemical or genetic interactions between HDAC6 and BBS proteins. However, HDAC6 has been indirectly implicated in cilia resorption (Pugacheva

et al., 2007). Conceivably, a subunit of the BBSome could inhibit axonemal MT deacetylation, thereby preventing premature cilia disassembly driven by HDAC6. We have previously reported an uncoupling between axonemal tubulin acetylation and ciliary membrane growth upon Rab8-GTP expression (Nachury et al., 2007). An appealing hypothesis is that the BBSome may couple ciliary membrane growth with axoneme acetylation.

EXPERIMENTAL PROCEDURES

Antibodies and Reagents

Antibodies were raised in rabbits against recombinant GST-BBIP10 and affinity purified on a His-BBIP10 column by using standard protocols. Antibodies against BBS4 and PCM-1 were previously published (Dammermann and Merdes, 2002; Nachury et al., 2007). GT335 antibody was provided courtesy of C. Janke. Centrin antibody was a gift from J. Salisbury. Commercial antibodies were against tyrosinated α-tubulin (YL1/2), α-tubulin (DM1A), Glu-tubulin (Chemicon), polyglutamylated tubulin (B3), acetylated α-tubulin (mAb 6-11B-1), rabbit pericentrin (ab4448, Novus), and GFP (3E6, Invitrogen). Purified bovine brain tubulin and rhodamine-tubulin were purchased from Cytoskeleton. Tubacin and niltubacin were provided courtesy of R. Mazitschek (Broad Institute, ICG-NCI). All chemicals were purchased from Sigma-Aldrich unless otherwise noted.

Plasmids and Proteins

BBIP10 was amplified from pCMV-SPORT6 (IMAGE clone ID 6063114) and subcloned into pDONR221 (Invitrogen). BBIP10 expression constructs were generated by Gateway subcloning into pcDNA3.1-nV5, pDEST53, pDEST17, pDEST15 (Invitrogen), or pCS2+Myc. An siRNA-resistant version of BBIP10 was synthesized by DNA 2.0, Inc. in the Gateway vector pDONR221 and subcloned into pDEST53 (Invitrogen). HDAC6 and HDAC1 clones were obtained from an in-house full-length cDNA collection and subcloned into pDEST53 vector. GST-BBIP10 was expressed and purified by using standard methods. His-BBIP10 was purified on Ni-Agarose under denaturing conditions and refolded overnight by dilution. Synthetic mRNA was transcribed with SP6 by using the Ambion mMESSAGE mMACHINE high-yield capped RNA kit.

Cell Culture, Transfections, and Quantitative RT-PCR

A stable RPE-hTERT cell line expressing LAP-BBS4 was previously described by Nachury et al. (2007). A U-205 cell line stably expressing RFP-α-tubulin was purchased from Marinpharm Gbmh. Control nontargeting siRNA #1 from Dharmacon was used as control siRNA in all experiments. Four siRNA duplexes against each BBS gene were synthesized in-house following Dharmacon siGenome sequences. The most potent siRNA duplex was selected after assessment of mRNA knockdown by qRT-PCR. For qRT-PCR, total RNA was prepared with the RNeasy Mini kit (QIAGEN).RNA (100 ng) was used for qRT-PCR by using the QuantiTech RT-PCR kit (QIAGEN). Triplicate reactions were run and analyzed on an ABI 7500 thermocycler. Sequences are available upon request. siRNA oligos against PCM-1 have been published (Dammermann and Merdes, 2002). Parental RPE or RPE-[^{LAP}BBS4] cells were plated on coverslips and transfected with 100 nM siRNA duplexes by using Lipofectamine RNAiMAX (Invitrogen) and by following the manufacturer's instructions. Cells were shifted from 10% serum to 0.2% serum 24 hr after transfection to induce ciliation, and they were fixed 48 to 72 hr posttransfection. Plasmids were transfected into RPE cells by using Fugene 6 (Roche), and cells were fixed 48 hr posttransfection.

Immunofluorescence and Microscopy

Fluorescent secondary antibodies were purchased from Jackson ImmunoResearch or Invitrogen. Immunofluorescence was performed according to standard protocols after fixation in 4% PFA (cilia staining) or in −20°C methanol (MT staining). Images were acquired on an Everest deconvolution workstation (Intelligent Imaging Innovations) equipped with a Zeiss AxioImager.Z1 microscope and a CoolSnapHQ-cooled CCD camera (Roper Scientific) and a 63× PlanApochromat, NA 1.4 objective. Between 10 and 16 z sections at 0.3 mm intervals were acquired, and z stacks were deconvolved and projected by using Slidebook 4.2 software (Intelligent Imaging Innovation). Contrasts were adjusted identically for each series of panels. Live-cell confocal microscopy was performed by using the Marianas inverted microscope system (Intelligent Imaging Innovations, Inc.) equipped with a Zeiss Axiovert 200M microscope, a Yokogawa SD-22 spinning disk confocal unit, a Cascade 512B camera, a laser ablation system (Photonic Instruments, Inc.), an environmental control chamber, and a Zeiss 63× (NA 1.4) PlanApochromat objective.

Tandem Affinity Purification, Biochemical Fractionations, and Mass Spectrometry

Purification of the LAP-BBS4 complexes was performed according to Nachury (2008). MTEV protease-eluted partially purified BBSome was fractionated on a 10%–40% linear sucrose gradient as described in Nachury (2008). To fractionate total RPE cell extracts, cells were lysed in LAP150 buffer (50 mM HEPES [pH 7.4], 150 mM KCl, 1 mM EGTA, 1 mM MgCl2, protease inhibitors) containing 0.3% NP-40, followed by centrifugation at 100,000 × g for 1 hr. The resulting extract was fractionated on a Superose-6 10/300 GL column (GE Healthcare), and fractions were concentrated by methanol/chloroform precipitation before SDS-PAGE electrophoresis and western blot. For the BBSome assembly assay, RPE-[^{LAP}BBS4] cells were transfected with siRNA duplex for 48 hr and incubated with labeling media (DMEM lacking L-Cysteine and L-Methionine [Invitrogen], with 10% dialyzed FBS, 1 mM glutamine, 1.5 mg/L L-methionine, 3 mg/L L-cysteine, 31.2 μCi/ml L-[^{35}S] in vitro Cell Labeling Mix [GE Healthcare]) for 16 hr. Labeled cells were harvested, and the BBSome was purified as described above, separated on SDS-PAGE, transferred to PVDF membrane, and exposed to Storage Phosphor Screen (GE Healthcare).

Microtubule Pelleting Assays

To measure relative levels of polymerized and soluble tubulin, siRNA-transfected cells were processed according to Minotti et al. (1991) to obtain a soluble protein fraction (S) and a cytoskeleton fraction (P). Equal volumes of S and P fractions were analyzed by quantitative western blot by using Cy5-labeled secondary antibodies (Jackson ImmunoResearch). Fraction volumes across different siRNA transfections were normalized based on protein concentration. MT copelleting and nucleation assays were performed according to Schatz et al. (2003).

Analysis of KV and the Melanosome Transport Assay

Zebrafish embryos were injected with ~6–10 nl volumes at the 1- to 8-cell stage, and phenotypic assays were performed according to Yen et al. (2006) by following a double-blind protocol isolating the personnel performing the injection from the personnel performing the phenotype scoring. BBIP10-ATG MO (5′-GAAACATTGACTTCACCTCCGGCAT-3′) injection mix concentrations ranged from 125 to 500 μM. BBS1 and 4 MOs are as described in Tayeh et al. (2008). Rescue of knockdown phenotypes were performed by using morpholino-resistant BBIP10 RNA obtained by cDNA subcloning into the pCS2+ expression vector.

ACCESSION NUMBERS

Nucleotide and protein sequences for BBIP10 are available at the National Center for Biotechnology Information (NR_015402) and UniProt (A8MTZ0).

SUPPLEMENTAL DATA

Supplemental Data include twelve figures, three movies, and Supplemental References and can be found with this article online at http://www.cell.com/developmentalcell/supplemental/S1534-5807(08)00473-5/.

ACKNOWLEDGMENTS

We thank Andreas Merdes for the PCM-1 antibody, Jeff Salisbury for the centrin antibody, Carsten Janke for the GT335 antibody, and R. Mazitschek for tubacin and niltubacin. Experiments with these compounds were performed in the M.V.N. laboratory (Stanford University). We are grateful to William Lane and the Harvard Microchemistry Facility for outstanding LC-MS/MS analysis and to Eric Chen of Intelligent Imaging Innovations, Inc. for help with microscopy. We thank Chris Westlake, Suzie Scales, and members of the P.K.J. laboratory

for critical review of the manuscript and for stimulating discussions. T.E.S. was supported by a Career Development Award from Research to Prevent Blindness. V.C.S. and P.K.J. acknowledge National Institutes of Health support (R01 EY11298 to V.C.S. and R01 GM073023 to P.K.J.). V.C.S is an investigator of the Howard Hughes Medical Institute. A.V.L., J.S.B., and P.K.J. are employees of Genentech, Inc.

Received: April 25, 2008
Revised: August 25, 2008
Accepted: November 4, 2008
Published: December 8, 2008

REFERENCES

Badano, J.L., Mitsuma, N., Beales, P.L., and Katsanis, N. (2006). The ciliopathies: an emerging class of human genetic disorders. Annu. Rev. Genomics Hum. Genet. *7*, 125–148.

Berbari, N.F., Lewis, J.S., Bishop, G.A., Askwith, C.C., and Mykytyn, K. (2008). Bardet-Biedl syndrome proteins are required for the localization of G protein-coupled receptors to primary cilia. Proc. Natl. Acad. Sci. USA *105*, 4242–4246.

Blacque, O.E., and Leroux, M.R. (2006). Bardet-Biedl syndrome: an emerging pathomechanism of intracellular transport. Cell. Mol. Life Sci. *63*, 2145–2161.

Bobinnec, Y., Khodjakov, A., Mir, L.M., Rieder, C.L., Edde, B., and Bornens, M. (1998). Centriole disassembly in vivo and its effect on centrosome structure and function in vertebrate cells. J. Cell Biol. *143*, 1575–1589.

Bonnet, C., Boucher, D., Lazereg, S., Pedrotti, B., Islam, K., Denoulet, P., and Larcher, J.C. (2001). Differential binding regulation of microtubule-associated proteins MAP1A, MAP1B, and MAP2 by tubulin polyglutamylation. J. Biol. Chem. *276*, 12839–12848.

Chiang, A.P., Beck, J.S., Yen, H.J., Tayeh, M.K., Scheetz, T.E., Swiderski, R.E., Nishimura, D.Y., Braun, T.A., Kim, K.Y., Huang, J., et al. (2006). Homozygosity mapping with SNP arrays identifies TRIM32, an E3 ubiquitin ligase, as a Bardet-Biedl syndrome gene (BBS11). Proc. Natl. Acad. Sci. USA *103*, 6287–6292.

Christensen, S.T., and Ott, C.M. (2007). Cell signaling. A ciliary signaling switch. Science *317*, 330–331.

Corbit, K.C., Aanstad, P., Singla, V., Norman, A.R., Stainier, D.Y., and Reiter, J.F. (2005). Vertebrate Smoothened functions at the primary cilium. Nature *437*, 1018–1021.

Dammermann, A., and Merdes, A. (2002). Assembly of centrosomal proteins and microtubule organization depends on PCM-1. J. Cell Biol. *159*, 255–266.

Davis, R.E., Swiderski, R.E., Rahmouni, K., Nishimura, D.Y., Mullins, R.F., Agassandian, K., Philp, A.R., Searby, C.C., Andrews, M.P., Thompson, S., et al. (2007). A knockin mouse model of the Bardet-Biedl syndrome 1 M390R mutation has cilia defects, ventriculomegaly, retinopathy, and obesity. Proc. Natl. Acad. Sci. USA *104*, 19422–19427.

Eisen, M.B., Spellman, P.T., Brown, P.O., and Botstein, D. (1998). Cluster analysis and display of genome-wide expression patterns. Proc. Natl. Acad. Sci. USA *95*, 14863–14868.

Fath, M.A., Mullins, R.F., Searby, C., Nishimura, D.Y., Wei, J., Rahmouni, K., Davis, R.E., Tayeh, M.K., Andrews, M., Yang, B., et al. (2005). Mkks-null mice have a phenotype resembling Bardet-Biedl syndrome. Hum. Mol. Genet. *14*, 1109–1118.

Gaertig, J., Cruz, M.A., Bowen, J., Gu, L., Pennock, D.G., and Gorovsky, M.A. (1995). Acetylation of lysine 40 in α-tubulin is not essential in *Tetrahymena thermophila*. J. Cell Biol. *129*, 1301–1310.

Gagnon, C., White, D., Cosson, J., Huitorel, P., Edde, B., Desbruyeres, E., Paturle-Lafanechere, L., Multigner, L., Job, D., and Cibert, C. (1996). The polyglutamylated lateral chain of α-tubulin plays a key role in flagellar motility. J. Cell Sci. *109*, 1545–1553.

Graser, S., Stierhof, Y.D., and Nigg, E.A. (2007). Cep68 and Cep215 (Cdk5rap2) are required for centrosome cohesion. J. Cell Sci. *120*, 4321–4331.

Haggarty, S.J., Koeller, K.M., Wong, J.C., Grozinger, C.M., and Schreiber, S.L. (2003). Domain-selective small-molecule inhibitor of histone deacetylase 6 (HDAC6)-mediated tubulin deacetylation. Proc. Natl. Acad. Sci. USA *100*, 4389–4394.

Huangfu, D., Liu, A., Rakeman, A.S., Murcia, N.S., Niswander, L., and Anderson, K.V. (2003). Hedgehog signalling in the mouse requires intraflagellar transport proteins. Nature *426*, 83–87.

Hubbert, C., Guardiola, A., Shao, R., Kawaguchi, Y., Ito, A., Nixon, A., Yoshida, M., Wang, X.F., and Yao, T.P. (2002). HDAC6 is a microtubule-associated deacetylase. Nature *417*, 455–458.

Johnson, K.A. (1998). The axonemal microtubules of the *Chlamydomonas* flagellum differ in tubulin isoform content. J. Cell Sci. *111*, 313–320.

Jurczyk, A., Gromley, A., Redick, S., San Agustin, J., Witman, G., Pazour, G.J., Peters, D.J., and Doxsey, S. (2004). Pericentrin forms a complex with intraflagellar transport proteins and polycystin-2 and is required for primary cilia assembly. J. Cell Biol. *166*, 637–643.

Kim, J.C., Badano, J.L., Sibold, S., Esmail, M.A., Hill, J., Hoskins, B.E., Leitch, C.C., Venner, K., Ansley, S.J., Ross, A.J., et al. (2004). The Bardet-Biedl protein BBS4 targets cargo to the pericentriolar region and is required for microtubule anchoring and cell cycle progression. Nat. Genet. *36*, 462–470.

Kim, J.C., Ou, Y.Y., Badano, J.L., Esmail, M.A., Leitch, C.C., Fiedrich, E., Beales, P.L., Archibald, J.M., Katsanis, N., Rattner, J.B., et al. (2005). MKKS/BBS6, a divergent chaperonin-like protein linked to the obesity disorder Bardet-Biedl syndrome, is a novel centrosomal component required for cytokinesis. J. Cell Sci. *118*, 1007–1020.

Kozminski, K.G., Diener, D.R., and Rosenbaum, J.L. (1993). High level expression of nonacetylatable α-tubulin in *Chlamydomonas reinhardtii*. Cell Motil. Cytoskeleton *25*, 158–170.

Lippincott-Schwartz, J., Cole, N.B., Marotta, A., Conrad, P.A., and Bloom, G.S. (1995). Kinesin is the motor for microtubule-mediated Golgi-to-ER membrane traffic. J. Cell Biol. *128*, 293–306.

Maruta, H., Greer, K., and Rosenbaum, J.L. (1986). The acetylation of α-tubulin and its relationship to the assembly and disassembly of microtubules. J. Cell Biol. *103*, 571–579.

Mikule, K., Delaval, B., Kaldis, P., Jurcyzk, A., Hergert, P., and Doxsey, S. (2007). Loss of centrosome integrity induces p38-p53-p21-dependent G1-S arrest. Nat. Cell Biol. *9*, 160–170.

Minotti, A.M., Barlow, S.B., and Cabral, F. (1991). Resistance to antimitotic drugs in Chinese hamster ovary cells correlates with changes in the level of polymerized tubulin. J. Biol. Chem. *266*, 3987–3994.

Mykytyn, K., Mullins, R.F., Andrews, M., Chiang, A.P., Swiderski, R.E., Yang, B., Braun, T., Casavant, T., Stone, E.M., and Sheffield, V.C. (2004). Bardet-Biedl syndrome type 4 (BBS4)-null mice implicate Bbs4 in flagella formation but not global cilia assembly. Proc. Natl. Acad. Sci. USA *101*, 8664–8669.

Nachury, M.V. (2008). Tandem affinity purification of the BBSome, a critical regulator of Rab8 in ciliogenesis. Methods Enzymol. *439*, 501–513.

Nachury, M.V., Loktev, A.V., Zhang, Q., Westlake, C.J., Peranen, J., Merdes, A., Slusarski, D.C., Scheller, R.H., Bazan, J.F., Sheffield, V.C., et al. (2007). A core complex of BBS proteins cooperates with the GTPase Rab8 to promote ciliary membrane biogenesis. Cell *129*, 1201–1213.

Nishimura, D.Y., Fath, M., Mullins, R.F., Searby, C., Andrews, M., Davis, R., Andorf, J.L., Mykytyn, K., Swiderski, R.E., Yang, B., et al. (2004). Bbs2-null mice have neurosensory deficits, a defect in social dominance, and retinopathy associated with mislocalization of rhodopsin. Proc. Natl. Acad. Sci. USA *101*, 16588–16593.

North, B.J., Marshall, B.L., Borra, M.T., Denu, J.M., and Verdin, E. (2003). The human Sir2 ortholog, SIRT2, is an NAD^+-dependent tubulin deacetylase. Mol. Cell *11*, 437–444.

Ou, G., Blacque, O.E., Snow, J.J., Leroux, M.R., and Scholey, J.M. (2005). Functional coordination of intraflagellar transport motors. Nature *436*, 583–587.

Ou, G., Koga, M., Blacque, O.E., Murayama, T., Ohshima, Y., Schafer, J.C., Li, C., Yoder, B.K., Leroux, M.R., and Scholey, J.M. (2007). Sensory ciliogenesis in *Caenorhabditis elegans*: assignment of IFT components into distinct modules based on transport and phenotypic profiles. Mol. Biol. Cell *18*, 1554–1569.

Palazzo, A., Ackerman, B., and Gundersen, G.G. (2003). Cell biology: tubulin acetylation and cell motility. Nature *421*, 230.

Piperno, G., LeDizet, M., and Chang, X.J. (1987). Microtubules containing acetylated α-tubulin in mammalian cells in culture. J. Cell Biol. *104*, 289–302.

Pugacheva, E.N., Jablonski, S.A., Hartman, T.R., Henske, E.P., and Golemis, E.A. (2007). HEF1-dependent Aurora A activation induces disassembly of the primary cilium. Cell *129*, 1351–1363.

Reed, N.A., Cai, D., Blasius, T.L., Jih, G.T., Meyhofer, E., Gaertig, J., and Verhey, K.J. (2006). Microtubule acetylation promotes kinesin-1 binding and transport. Curr. Biol. *16*, 2166–2172.

Rohatgi, R., Milenkovic, L., and Scott, M.P. (2007). Patched1 regulates hedgehog signaling at the primary cilium. Science *317*, 372–376.

Schatz, C.A., Santarella, R., Hoenger, A., Karsenti, E., Mattaj, I.W., Gruss, O.J., and Carazo-Salas, R.E. (2003). Importin α-regulated nucleation of microtubules by TPX2. EMBO J. *22*, 2060–2070.

Scheetz, T.E., Kim, K.Y., Swiderski, R.E., Philp, A.R., Braun, T.A., Knudtson, K.L., Dorrance, A.M., DiBona, G.F., Huang, J., Casavant, T.L., et al. (2006). Regulation of gene expression in the mammalian eye and its relevance to eye disease. Proc. Natl. Acad. Sci. USA *103*, 14429–14434.

Scholey, J.M., and Anderson, K.V. (2006). Intraflagellar transport and cilium-based signaling. Cell *125*, 439–442.

Sheffield, V.C., Heon, E., Stone, E.M., and Carmi, R. (2004). BBS genes and the Bardet-Biedl syndrome. In Inborn Errors of Development, P.R.E.C.C. Epstein and A. Wynshaw-Boris, eds. (Oxford: Oxford University Press), pp. 1044–1049.

Takemura, R., Okabe, S., Umeyama, T., Kanai, Y., Cowan, N.J., and Hirokawa, N. (1992). Increased microtubule stability and α tubulin acetylation in cells transfected with microtubule-associated proteins MAP1B, MAP2 or tau. J. Cell Sci. *103*, 953–964.

Tayeh, M.K., Yen, H.J., Beck, J.S., Searby, C.C., Westfall, T.A., Griesbach, H., Sheffield, V.C., and Slusarski, D.C. (2008). Genetic interaction between Bardet-Biedl syndrome genes and implications for limb patterning. Hum. Mol. Genet. *17*, 1956–1967.

Vale, R.D., Reese, T.S., and Sheetz, M.P. (1985). Identification of a novel force-generating protein, kinesin, involved in microtubule-based motility. Cell *42*, 39–50.

Verhey, K.J., and Gaertig, J. (2007). The tubulin code. Cell Cycle *6*, 2152–2160.

Webster, D.R., Gundersen, G.G., Bulinski, J.C., and Borisy, G.G. (1987). Differential turnover of tyrosinated and detyrosinated microtubules. Proc. Natl. Acad. Sci. USA *84*, 9040–9044.

Westermann, S., and Weber, K. (2003). Post-translational modifications regulate microtubule function. Nat. Rev. Mol. Cell Biol. *4*, 938–947.

Yen, H.J., Tayeh, M.K., Mullins, R.F., Stone, E.M., Sheffield, V.C., and Slusarski, D.C. (2006). Bardet-Biedl syndrome genes are important in retrograde intracellular trafficking and Kupffer's vesicle cilia function. Hum. Mol. Genet. *15*, 667–677.

Zhang, Y., Kwon, S., Yamaguchi, T., Cubizolles, F., Rousseaux, S., Kneissel, M., Cao, C., Li, N., Cheng, H.L., Chua, K., et al. (2008). Mice lacking histone deacetylase 6 have hyperacetylated tubulin but are viable and develop normally. Mol. Cell. Biol. *28*, 1688–1701.